Macromolecules

ARTICLE

pubs.acs.org/Macromolecules

Mesogens Mediated Self-Assembly in Applications of Bulk Heterojunction Solar Cells Based on a Conjugated Polymer with Narrow Band Gap

Kai Yao,[†] Yiwang Chen,[*,†,‡] Lie Chen,[*,†] Fan Li,[*,†] Xuee Li,[†] Xingye Ren,[‡] Hongming Wang,[‡] and Tianxi Liu[§]

[†]Institute of Polymers, Nanchang University, 999 Xuefu Avenue, Nanchang 330031, China

[‡]Institute of Advanced Study, Nanchang University, 999 Xuefu Avenue, Nanchang 330031, China

[§]Department of Macromolecular Science, Fudan University, 220 Handan Road, Shanghai 200433, China

Supporting Information

ABSTRACT: The ability to control the molecular organization of electronically active liquid-crystalline polymer provides opportunities to develop easy-to-process yet highly ordered supramolecular systems in the field of photovoltaics. Here, we report a novel donor−acceptor type liquid-crystalline copolymer, poly{9,9-bis[6-(4′-cyanobiphenyloxy) hexyl]fluorene-*alt*-5,5-(4′,7′-di-2-thienyl-2′,1,3′-benzothiadiazole)}, PFcbpDTBT, which contains both electron-donating fluorene and electron-accepting benzothiadiazole units. Incorporating the electron withdrawing cyanobiphenyl units not only narrowed the band gap of the copolymer but also help main chain form spontaneously through self-organization. The films with structural anisotropy can endow the PFcbpDTBT with special features, including absorption band red-shift; fluorescence enhancement; lower lying LUMO level, and crystallinity improvement. When blended with PCBM, the PFcbpDTBT enables the acceptors to adopt the preferential well-oriented arrangement in both surface and inner of the bulk. Among all the thermal treatments, the mesophase annealing achieves the most obvious effect. From the device annealed at 200 °C, the internal quantum efficiency remains or exceeds 20% throughout the 400−650 nm spectrum and the power conversion efficiency values reaches 1.10% without extensive optimization.

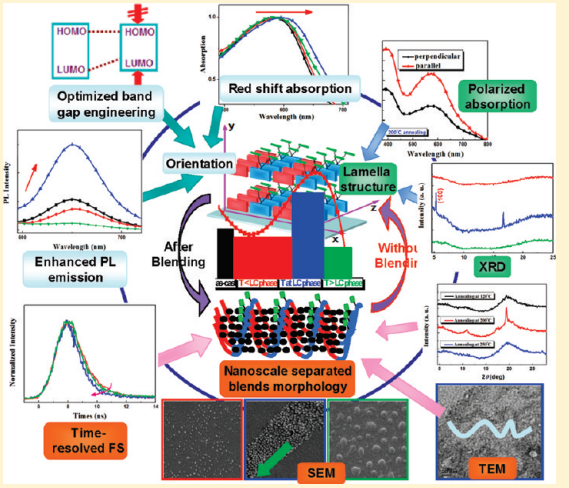

INTRODUCTION

Over the past few years, bulk heterojunction (BHJ) photovoltaic cells consisting of semiconducting polymers as donors mixed with fullerene derivatives as acceptors have emerged as a promising low-cost energy source. Because of their numerous advantages such as production on flexible and large-area substrates by solution processing, photovoltaic cells (PCs) can dramatically reduce the manufacturing costs.[1] Preliminary studies on polyfluorene derivative blends have revealed interesting photovoltaic effects that make them suitable to be used as donor components in BHJ solar cells.[2] To achieve a polymer solar cell device with a high light harvesting ability (low band gap) as well as a high open-circuit voltage, one feasible approach is to design alternating donor−acceptor copolymers based on polyfluorene, where the fluorene unit may provide a deeper HOMO level and the electron acceptor unit is used to tune the electronic band gap of the polymers.[3] In 2003, Andersson et al. reported for the first time an efficient and promising BHJ solar cell using a low band gap polyfluorene derivative (PFDTBT; Scheme1) that exhibited a PCE of 1.7%.[4] Up to now, the best solar cell based on polyfluorene derivatives was reported by Tsukamoto et al. with a V_{oc} = 0.99 V and PCE of 5.50%.[5]

The main factor heavily affecting the performance of PSC is the nanomorphology of the photoactive layer. Because of the short lifetime of the exciton, its diffusion length in organic materials is only about 10−20 nm.[6] This means that the exciton must reach the D/A interface to give the charge transfer without undergoing to a radiative or nonradiative decay. Thus, the donor and acceptor phases should self-organize to form nanodomains with dimensions comparable to the exciton diffusion length. To increase the possibility for the exciton to reach the interface, the donor−acceptor contact area must be as large as possible.[7] During the past years it has been widely demonstrated that the enhanced nanoscale phase morphologies can been achieved through different approaches, including postfabrication annealing at high temperature, additives, and slow film growth by

Received: January 26, 2011
Revised: March 6, 2011
Published: March 18, 2011

Scheme 1. Chemical Structure of PFDTBT and PFcbpDTBT[a]

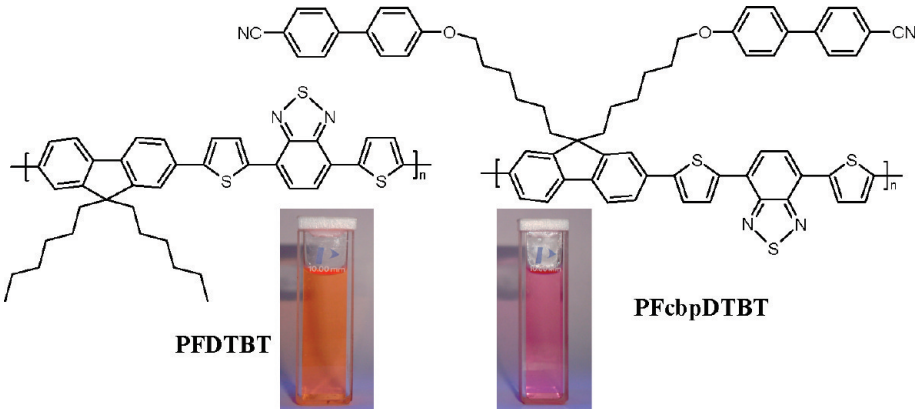

[a] The insets show the digital photographs of PFDTBT and PFcbpTBT in chlorobenzene (10^{-5} mol/L) at room temperature, under 365 nm excitation.

controlling the solvent evaporation rate of the active layer (so-called "solvent annealing").[8] Thermal treatments have profound effects on the blend morphology, and a lot of work has been carried out to characterize the evolution of active layer morphology upon heating. Parallel to the relevant enhancement of cell performance, a remarkable effect of the annealing processes on the optical properties of the active layer is always observed.[9]

Liquid-crystalline (LC) polymer can self-assemble into a well-ordered nanostructure, and liquid-crystalline materials can facilitate the hole transport in active layer, particularly after thermal treatment in the mesophase.[10] This situation inspired us to design a polymer system with electron-accepting and electron-donating building blocks, that is, a donor−acceptor type alternating copolymer with liquid-crystalline side chain, to optimize processability, crystalline nanostructure, and control nanoscale morphology of active layer eventually. In our previous studies, we have synthesized liquid-crystalline polyfluorene derivates containing terphenyl mesogens with alkyl terminal group and found that the spontaneous assembly of the liquid-crystalline molecules pushes PCBM clusters to form an oriented nanodispersing structure.[11]

Here, by introducing the cyanobiphenyl mesogens into PFDTBT, we designed a new donor−acceptor type copolymer (see Scheme 1), poly{9,9-bis[6-(4′-cyanobiphenyloxy)hexyl] fluorene-*alt*-5,5-(4′,7′-di-2-thienyl-2′,1′,3′-benzothiadiazole)}, PFcbpDTBT, via copolymerization of liquid-crystalline electron-donating fluorene and electron-accepting dithienylbenzothiadiazole (DTBT) units. The self-assemble mesogens could induce and enhance the orientation degree of the active layer. Although cyano terminal group is distant from the conjugated backbone and separated by the saturated bridge, the strong electron-withdrawing effect could lower molecular orbital levels of the polymer to increase the absorption of the solar spectrum to some extent.[12] The synthetic route to PFcbpDTBT is depicted in Figure S1 (see Supporting Information), and the synthesis of high molecular weight, readily soluble copolymers is accomplished by Pd-catalyzed Suzuki coupling reactions.

RESULTS AND DISCUSSION

The structure of PFcbpDTBT was confirmed by ^{1}H NMR, ^{13}C NMR, FT-IR, and elemental analysis. The presence of the cyano functionality is confirmed by the appearance of FT-IR bands at 2230 cm^{-1} (see Supporting Information, Figure S1). The ^{1}H NMR of PFcbpDTBT is here compared with that of PFDTBT to illustrate the polymer structure (Scheme 1). Two signals (7.60 and 3.83 ppm) are evident from the protons on the cyanobiphenyl rings and methylene for oxygen (CH_2−O), respectively (Figures S2 and S3). The ^{13}C NMR spectrum of the copolymer also agrees with the molecular structures, and all other resonance peaks can be readily assigned with no unexpected signals found (see Figure S3 in the Supporting Information).

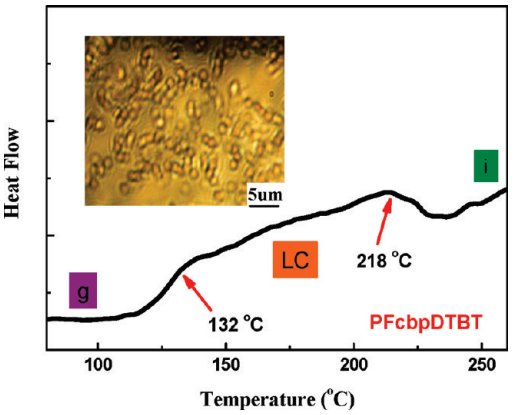

Figure 1. DSC thermogram of the copolymer recorded under nitrogen during second heating scans at a scan rate of 20 °C/min. The mesomorphic textures observed by POM at 200 °C under cooling from melt state (cooling rate: 1 °C/min).

The polymer is thermally stable and almost loses no weight at temperature as high as 380 °C in the thermogravimetric analysis, which is ascribed to the mesogenic appendages well wrapping the conjugated backbone to protect them from the perturbations by heat and attacks by the degradative species. (Figure S4). The mesomorphic behavior of PFcbpDTBT also has been studied by polarizing optical microscopy (POM) and differential scanning calorimetry (DSC) (Figure 1). Observed by POM, enantiotropic optical anisotropy with batonnet-like structure of the copolymer emerges from the dark background when heated or cooled, suggesting the nature of liquid-crystalline phase. At the same time, polymer PFcbpDTBT exhibits two discrete endotherm transitions at 132 and 218 °C on second heating scan in DSC

dx.doi.org/10.1021/ma200179u |*Macromolecules* 2011, 44, 2698–2706

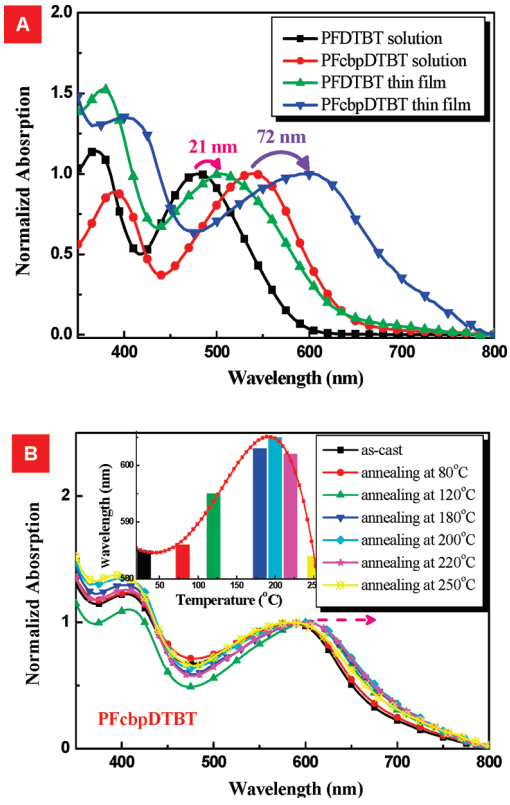

Figure 2. UV−vis absorption spectra of copolymers in CB solution and in solid state of copolymer PFDTBT and PFcbpDTBT (A). UV−vis absorption spectra of film PFcbpDTBT under different temperature annealing on a quartz plate (B). The inset histogram shows the shift of the maximum absorptions at long band after various thermal annealings.

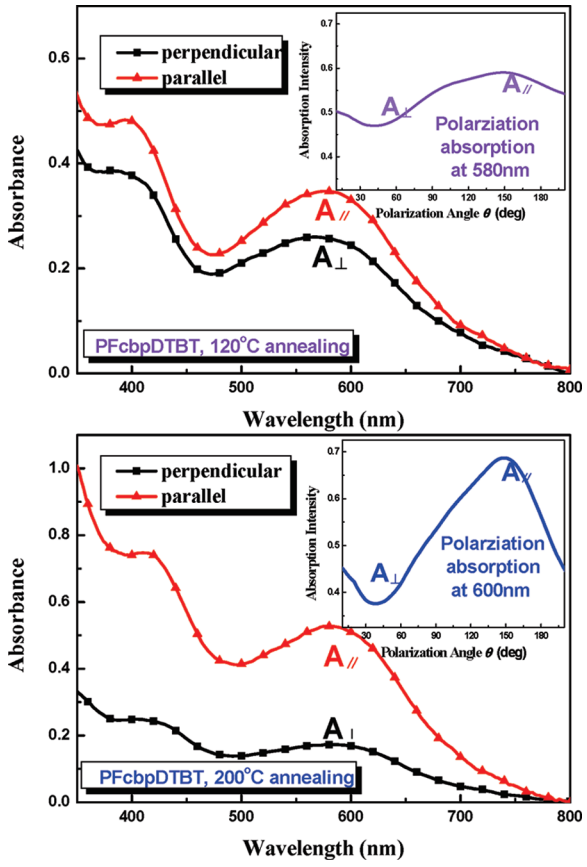

Figure 3. UV−vis absorption spectra of the polymer film annealed at 120 °C (up) and 200 °C (down) on a quartz plate with linearly polarized incident light at parrallel or perpendicular to the long aixs of the molecule direction. The insets shows the polarized absorption for film annealed at 120 °C (580 nm) and 200 °C (600 nm).

curves and two exothermic transitions at 130 and 215 °C on cooling. The first transition corresponds to the solid−mesophase transition, and the second corresponds to the mesophase−isotropic transition. The liquid-crystalline property and the packing arrangement of molecules also can be supported by XRD analysis (discussed later).

The UV−vis absorption peaks of crystalline π-conjugated polymer films are usually red-shifted relative to those measured in solution. This behavior is due to the enhanced intermolecular interactions between the polymer chains and the planarization effect of the π-conjugated polymer backbone, which enable the polymer chains to self-assemble into a well-ordered nanostructure in the solid state.[13] The extent of the red shift is related to the degree of order in the polymer; for example, the red shift can be up to 70 nm for some regioregular π-conjugated polymers, such as HT-P3HT (head−tail), whereas there is only a small shift or no shift at all for others, such as HH-P3HT (head−head).[14] Figure 2a shows the normalized UV−vis absorption spectra of PFDTBT and PFcbpDTBT in a chlorobenzene (CB) solution and in the solid state. Interestingly, whatever state it is, the PFcbpDTBT containing cyanobiphenyl shows red-shifted absorption bands than the pristine PFDTBT. The absorption peaks corresponding to the $\pi-\pi^*$ transitions of the polymer PFcbpDTBT in the solution and solid phase (annealing at 200 °C) are present at 533 and 605 nm, respectively. This large red shift (72 nm) suggests the presence of strong interchain interactions. However, for the PFDTBT without attaching mesogens, the shift from the solution state to the thin film state is only 21 nm.

In addition, the effects of thermal annealing on PFcbpDTBT films were investigated using UV−vis absorption spectra (Figure 2b). A 20 mg/mL chlorobenzene solution of PFcbpDTBT was spin-coated to fabricate films that were subsequently annealed at 80, 120, 180, 200, 220, and 250 °C for 1 h under nitrogen. For the as-spin sample, the main absorption band of the PFcbpDTBT thin film is at 585 nm. Importantly, as the annealing temperature increased to 120 °C, the main absoroption peak red-shifts to 602 nm due to more oriented $\pi-\pi$ stacking.[15] These features became dramatically pronounced (20 nm red-shift) for samples annealed in the mesophase region (particular at 200 °C). However, when the annealing temperatures exceed the mesophase, it would disrupt the tendency and get worse results. The inset columnar figure in Figure 2b elaborates this phenomenon.

In order to study the molecular orientation under the thermal annealing of π-conjugated polymers in thin solid film, the structures of the thin films were investigated by measuring polarized absorption spectra. Through the polarization absorption (the insets in Figure 3) of the films annealed at 120 °C (580 nm) and 200 °C (600 nm) at their maximum absorption peaks, respectively, we can conclude the long axis of the molecule arrangement at 140° polarized angle. Figure 3 shows the absorption spectra of the cast film with the incident light linearly polarized light at parallel (at 140°) or perpendicular (at 50°) to the long axis direction. For the film annealed at low temperature

dx.doi.org/10.1021/ma200179u |*Macromolecules* 2011, 44, 2698–2706

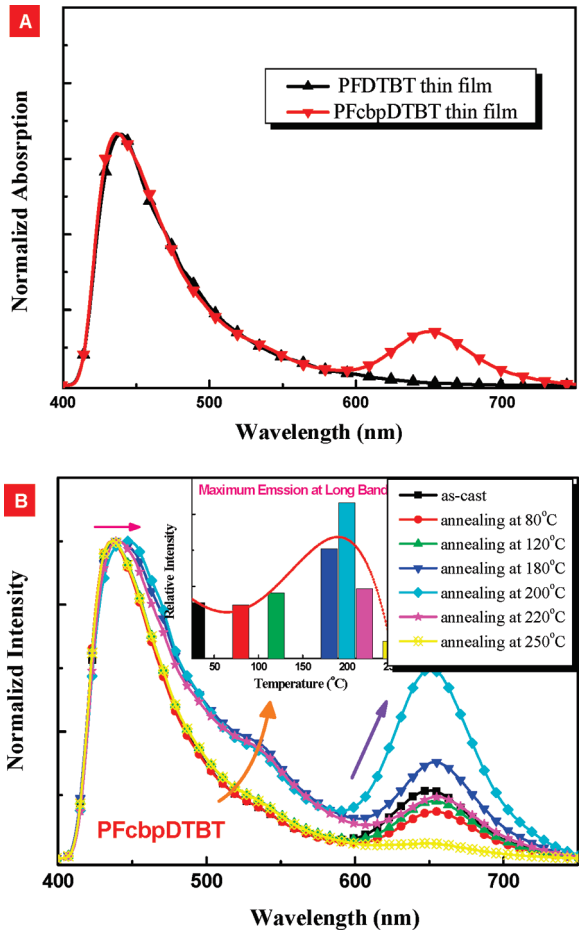

Figure 4. Fluorescence spectra of copolymers in solid state of copolymer PFDTBT and PFcbpDTBT (A). Fluorescence spectra of PFcbpDTBT film under different temperature annealing on a quartz plate (B). The inset histogram shows the relative intensity of the maximum emissions at long band after various thermal annealing (λ_{ex} = 300 nm).

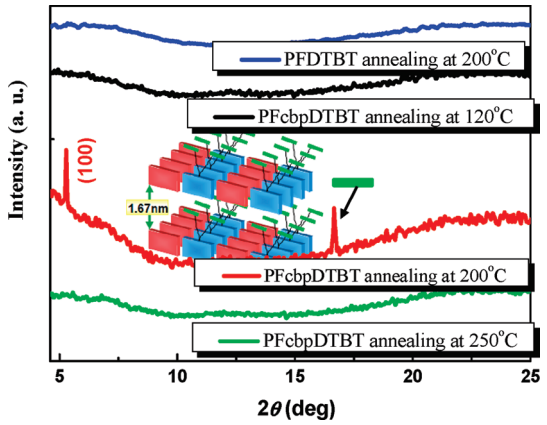

Figure 5. X-ray diffraction patterns PFcbpDTBT films at different treatments. The inset shows the lamella structure of the copolymer in mesogenic state. The PFDTBT film annealed at 200 °C is added for comparison.

(120 °C), the absorption curves shows tiny increase when the light was parallel, while the much stronger absorption was observed under the parallel direction after mesophase annealing (200 °C). The dichroic ration ($A_{\parallel}/A_{\perp}$) at the maximum absorption of long wavenumber of the films annealed at 120 and 200 °C (at LC state) changed from 1.31 to 3.12, respectively. These results indicate that the LC thermal treatment promote the uniaxially alignment of the molecule structure parallel to the long axis direction (details of orientation in the XRD data).[16]

The photoluminescent spectra of the polymers PFDTBT and PFcbpDTBT films, produced by excitation with the 300 nm, are presented in Figure 4A. For the copolymer PFcbpDTBT film, the emission peak at ca. 450 nm are attributed to the fluorene segment and the additional long wavelength absorption bands at ca. 650 nm are attributed to the DTBT unit in main chain,[17] while the absorption bands of the DTBT unit is disappeared in the solid state of PFDTBT. This is ascribed to the better conjugation of the backbone induced by mesogenic pendants. Moreover, the normalized solid-state photoluminescent spectra of the copolymer PFcbpDTBT upon different treatments are summarized in Figure 4B. The fluorescence intensity at 650 nm increases gradually with the increasing annealing temperature until 200 °C, which is below the observed mesophase−isotropic transition. And it also repeats the descending trend when the temperatures pass over the mesophase region into the isotropic state. The tendency in those spectra provides evidence of well-ordered molecular structure after thermal annealing, especially annealed at mesophase. Interestingly, the copolymer thin films exhibit a distinctive vibronic splitting with a strong shoulder near 530 nm, which is the consequence of polymer chains self-assemble induced by the cyanobiphenyl mesogens into a well-ordered nanostructure in the solid state.[18]

The microstructures of the polymer PFcbpDTBT thin films at different thermal treatments were studied using X-ray diffraction, and the PFDTBT film annealed at 200 °C is added for comparison (Figure 5). The XRD diffractogram of a powdery sample can be generally divided into the low-angle Bragg reflections at $2\theta \sim 3°$ corresponding to the layer spacing of molecular orientational order and the high-angle peaks at $2\theta \sim 20°$ associated with the two-dimensional arrangement of the mesogenic pendants within the layers. The appearance of a broad or sharp peak furnishes a qualitative indication of the degree of order.[19] The XRD diffractogram of PFcbpDTBT annealing (200 °C) at the liquid-crystalline state is obtained an obvious diffraction peak at 2θ = 5.28°, which corresponds to the layering distance (1.67 nm), between the sheets of PFcbpDTBT chains associated with the plane perpendicular to their longitudinal axes. The diffuse halo at 2θ = 17.1° is characteristic for the ordered cyanobiphenyl, and the d value (d = 0.531 nm) of 2θ = 17.1° is corresponding with the biphenyl mesogenic length in vertical orientation. However, there is only a low intensity and broadly diffuse peak in the high-angle area for PFDTBT and the films of PFcbpDTBT annealed at temperatures below or above mesophase. It implies that the formation of liquid-crystalline domains with well-ordered crystalline nanostructure could be induced by oriented cyanobiphenyl only after LC thermal annealing.[20] With the aid of the polarized optical absorption spectra and POM, the packing arrangements of liquid-crystalline copolymer adopt preferential well-ordered intermolecular $\pi-\pi$ lamella stacking (inset of Figure 5).[21]

To determine the relationship of the electrochemical property with thermal treatments and to arrive at the reduction and oxidation potential values of the polymer, cyclic votammograms (CV) were recorded (Figure S5). We found that the highest

dx.doi.org/10.1021/ma200179u |*Macromolecules* 2011, 44, 2698–2706

Table 1. Electrochemical Properties of the Copolymers

polymers	$E_{onset/ox}$ (eV)	$E_{onset/red}$ (eV)	HOMO (eV)	LUMO (eV)	E_g^{ec} (eV)[a]	E_g^{opc} (eV)[b]
PFDTBT	0.68	−1.30	−5.50	−3.52	1.98 (1.99)[c]	1.93
PFcbpDTBT	0.67	−1.09	−5.49	−3.73	1.76 (1.80)	1.74
PFcbpDTBT(120)[d]	0.66	−0.99	−5.48	−3.83	1.65	1.68
PFcbpDTBT(200)	0.65	−0.90	−5.47	−3.92	1.55	1.59
PFcbpDTBT(250)	0.66	−0.98	−5.48	−3.84	1.64	1.66

[a] Calculated from the absorption band edge of the copolymer films, $E_g = 1240/\lambda_{edge}$. [b] Calculated from $E_g = e(E_{onset/ox} - E_{onset/red})$. [c] Evaluated HOMO−LUMO energy gaps (E_g) using DFT at the B3LYP/6-31G(d,p) level of theory. [d] The number in parentheses following the copolymer represented as the annealing temperatures.

Figure 6. Location of band gap and band edges of HOMO and LUMO (vs vacuum) of PFcbpDTBT, PCBM, and PFDTBT (without mesogenic side chain). Data obtained from onset potentials in CV. The number in the bar next to the PFcbpDTBT is the annealing temperature.

occupied and lowest unoccupied molecular orbital (HOMO/LUMO) levels of the modified PFDTBT are significantly optimized. In comparison with the pristine PFDTBT (5.5 and 3.52 eV),[22] the LUMO level of polymer PFcbpDTBT significantly decreases, while its HOMO level keeps low and experiences little change, which also are proved by the results of the band gap calculated from the optical onsets (Table 1). It ensures that the donor polymer possesses the lower band gap and low-lying HOMO energy level to provide a large open-circuit voltage. With the reference, the map of HOMO and LUMO orbital of the copolymers are presented in Figure 6. It is worth to note that the treatment of LC annealing (200 °C) can lower the band gap than other heat processes, and the results of the various treatments exhibit the same tendency to our previous report.[11]

Moreover, the observation of the electronic properties can be better understood by analyzing the results obtained from density functional calculations. The electronic structures of the alternating polymer series (as isolated oligomers) were evaluated using DFT at the B3LYP/6-31G (d,p) level of theory.[23] The HOMO and LUMO energies and pictorial representations of the frontier molecular orbital of the PFDTBT and PFcbpDTBT oligomers ($n = 3$) are shown in Figure 7. For PFDTBT (without cyanobiphenyl substitution), the results indicate that the electron density of LUMO is mainly localized on the acceptor unit, while the electron density of HOMO is distributed over the conjugated molecule (both the acceptor unit and donor unit). However, for the copolymer with cyanobiphenyl side chain, the LUMO is delocalized to some degree on the whole DTBT and fluorene moieties, which leads to the more low-lying LUMO energy level of −3.30 eV. Meanwhile, the HOMO of the PFcbpDTBT is also localized on the whole molecule with a deep level (−5.10 eV).

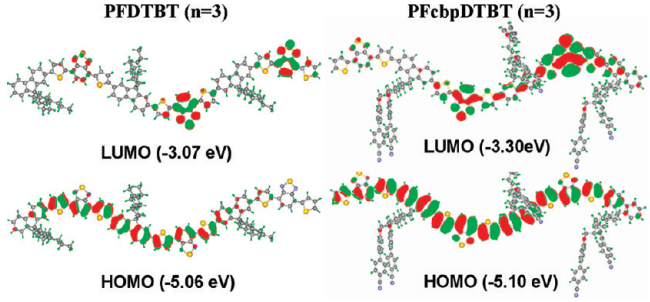

Figure 7. DFT-calculated LUMO and HOMO of the geometry-optimized structures of oligomers ($n = 3$) of PFDTBT (left) and PFcbpDTBT (right).

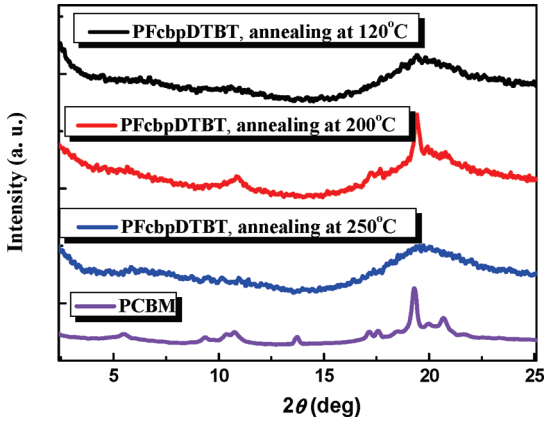

Figure 8. XRD spectra of PFcbpDTBT:PCBM (1:3 wt %) films at different treatments and pristine PCBM.

The trend of the calculated HOMO and LUMO energy levels and the difference (E_g) between them correlates well with that obtained from the electrochemical measurement (Table 1) and explains the reason for the reduce of the band gap after incorporating the cyanobiphenyl units. All of the observations suggest that the orientation degree of the polymer has been enhanced greatly by the mesogens, and the absorption band and energy levels of the resultant conjugated polymers have been fine-tuned by incorporation of the cyanobiphenyl group.

Thermal treatments have profound effects on the blend morphology of the active layer of the PCs, and a lot of work has been carried out to characterize the evolution of active layer morphology upon heating.[24] To investigate in detail the microstructure of the PFcbpDTBT:PCBM films at different thermal annealing temperatures, we first conducted X-ray diffraction of

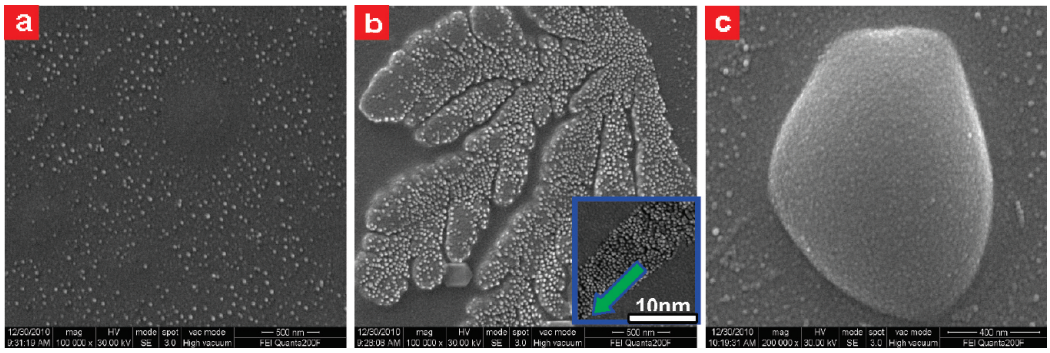

Figure 9. SEM topography of the PFcbpDTBT:PCBM (1:3 wt %) blend thin films spin-coated onto ITO/PEDOT substrate for various temperature annealing treatments: (a) 120 °C annealing, (b) 200 °C annealing (the inset shows the orientated direction), and (c) 250 °C annealing.

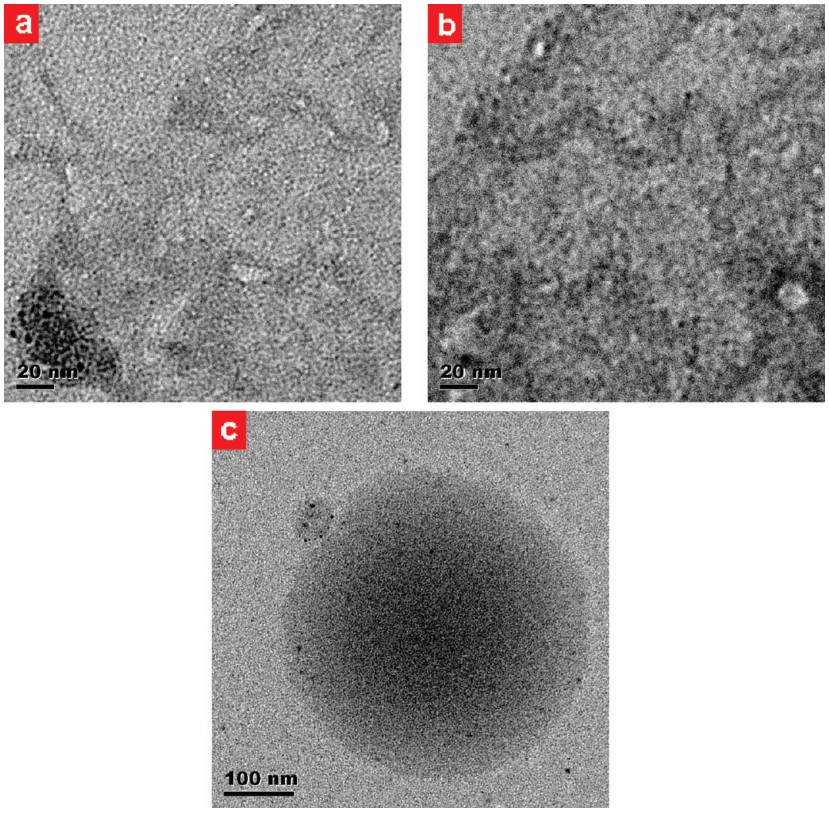

Figure 10. TEM images of the PFcbpDTBT:PCBM (1:3 wt %) blend films spin-cast from CB with increasing temperatures: (a) 120, (b) 200, and (c) 250 °C annealing.

the PFcbpDTBT:PCBM (1:3 wt %) films spin-coated on the ITO substrate (Figure 8). After the addition of the PFcbpDTBT, the crystallinity of the PCBM nanocrystals in the films annealed at 120 and 250 °C has been totally ruined, and the diffraction peaks caused by PCBM crystallites have not been detected. However, when the matrix is treated upon LC annealing at 200 °C, the crystallinity of the PCBM is significantly enhanced, indicating that the spontaneous assembly of the liquid-crystalline molecules pushes PCBM clusters to form oriented nanodispersing structure with highly oriented channel layers upon only heating at liquid-crystalline states.

The nanoscale morphologies of the PFcbpDTBT:$PC_{60}BM$ films were studied using top views scanning electron microscopy (SEM) and transmission electron microscopy (TEM). Because the exciton diffusion length is generally less than 10 nm, so the nanoscale phase separation in BHJ materials must be less than 20 nm.[25] The surface roughness and the size of these PCBM nanoclusters were shown in the topography images (Figure 9a−c). The annealing temperature impacts great influence on the nanoscale morphology of these blends. Particularly, the blends annealed at liquid-crystalline phase (200 °C) achieve the orientated (as the inset green arrow) nanoscale aggregated PCBM regions, which create phase separation interfaces for charge separation. However, when the temperature of annealing is increased to 250 °C, the phase separation domains are getting larger (over 200 nm) and decrease the charge separation

dx.doi.org/10.1021/ma200179u |*Macromolecules* 2011, 44, 2698–2706

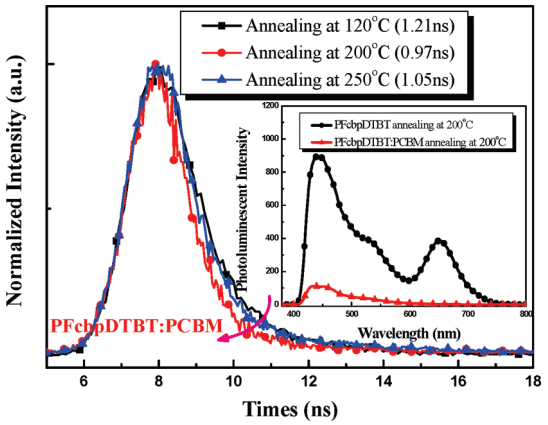

Figure 11. Photoluminescence lifetime decay of the PFcbpDTBT:PCBM blends (1:3) annealed at various temperatures, measured at the emission maximum of 650 nm with the λ_{ex} = 300 nm. The inset shows the photoluminescence spectra of the copolymer and blends annealed at mesophase (200 °C).

efficiency inversely.[26] The nanoscale phase separation for systems treated at low temperature (i.e., 120 °C) is too small to form effective percolated networks.

The morphology of the active layer was further verified by transmission electron microscopy (TEM). Parts a, b, and c of Figure 10 show the films annealed at 120, 200, and 250 °C, respectively, blended with PCBM as described. Relatively dark regions in the TEM image indicate PCBM-rich regions or aggregates.[27] For the blend annealed below mesophase, the interpenetrating networks are not well developed and the PCBM aggregation regions are very tiny. After thermal annealing at LC state for 1 h, a fully mixed morphology was formed, and the morphology of the interpenetrating donor−acceptor networks becomes clearer and easily visible. The intertwined and fibrous features (i.e., ∼5 nm width) suggest a better D−A interaction. However, once the annealed temperatures rise to 250 °C, isotropic polymers can leads to the bad aggregated PCBM. The large domins (about 200 nm diameter) prohibited the formation of percolated networks of the donor/acceptor blend and greatly surpassed the exciton diffusion length. It is clear that the nanoscale morphology of the blend films depends on the annealing temperature whether it falls in the LC state or not.

In order to get more careful investigation of the photophysics in the PFcbpDTBT:PCBM systems, we perform the time-resolved photoluminescence (TRPL) to see the exciton decay as a function of annealing temperature (shown in Figure 11). Very detailed studies of the transient optical absorption spectra of PFcbpDTBT:PCBM blends have been performed; the model describes the excitation, the formation of a bound polaron pair, and the subsequent geminate recombination of this polaron pair, with a lifetime of ∼30 ns.[28] Detected through the almost completely photoluminescence quenching (the inset of Figure 11), a conclusion is that the generation of photoinduced charge carriers are almost complete. The exciton lifetime decreases (from 1.21 to 0.97 ns) with increasing the annealing temperature before the mesophase−isotropic transition, which indicates the thermal process results in a favorable morphology. The favorable morphology increases the interface between polymer and PCBM, and the result is in good agreement with the results of the binary system morphology in TEM. For the blends annealed at 250 °C (over mesophase−isotropic transition), the poor morphology leads to a

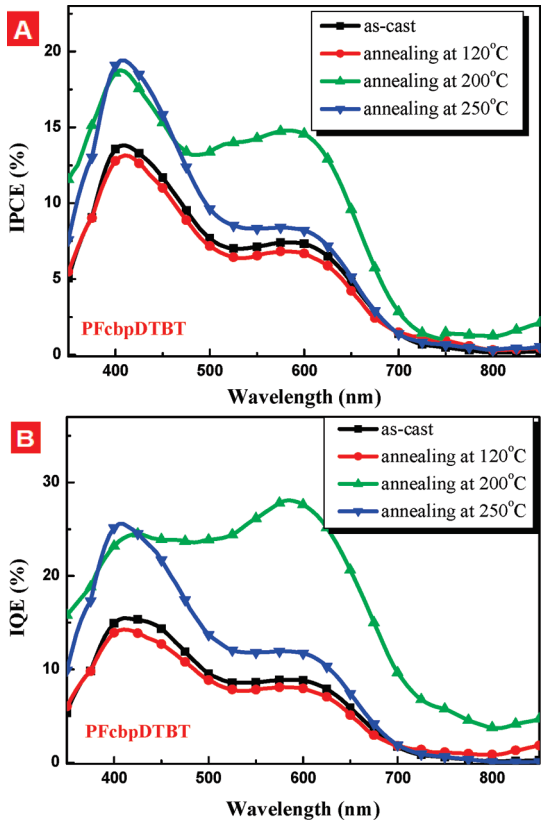

Figure 12. Incident photon-to-current efficiency (IPCE: A) and internal quantum efficiency (IQE: B) of photovoltaic cells calculated from the photocurrents under short-circuit conditions based on PFcbpDTBT:PCBM = 1:3 at different thermal treatments.

nonefficient charge separation and increase of the exciton lifetime from 0.97 to 1.05 ns. From these studies, we can demonstrate that liquid-crystalline thin films adopt preferential well-ordered stacking through the self-assembly of the polymer induced by the orientation of mesogen pendants.

The XRD, SEM, TEM, and TRPL analysis demonstrate that variations in the annealing conditions of PFcbpDTBT:PCBM system result in drastic changes in the molecular orientation, crystallinity, and nanoscale morphology of its thin films. Further, bulk heterojunction photovoltaic devices were constructed to investigate the influence on photovoltaic properties introduced by the liquid-crystalline side chains. For fair comparison, care was taken during the processing to maintain similarly structured devices: (a) all polymers were blended with PCBM at 1:3 weight ratio in CB at 20 mg/mL; (b) identical spin rate (1200 rpm) and time (1 min) were employed to achieve similar film thicknesses. The PSCs, which had the layered configuration of glass/ITO/PEDOT:PSS/PFcbpDTBT:PCBM/LiF/Al, were fabricated using established methods (Supporting Information).[29]

Figure 12A shows the incident photon-to-current efficiency (IPCE) spectra of solar cells comprising BHJ films treated under various annealing temperatures by monochromatic light. The shape of the IPCE curves of the device is very similar to the absorption spectra, showing two maxima. It indicates that all the absorption of the polymers contributed to the photovoltaic conversion. To be specific, the device without any treatment possesses two peak values of ∼13% and ∼8% at a wavelength of 410 and 580 nm, respectively. After annealing treated at 120 °C,

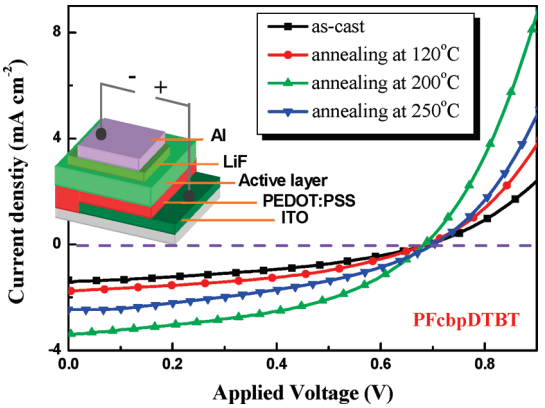

Figure 13. $J-V$ characteristics of photovoltaic cells based on PFcbpDTBT:PCBM = 1:3 at different thermal treatments under AM 1.5G illumination from a calibrated solar simulator with an intensity of 100 mW/cm^2. Inset is a schematic of device architecture.

the IPCE of the solar cell hardly shows obvious change compared with the as-cast one. However, when the annealing temperature rises to the mesophase (200 °C), the IPCE value is almost doubled to 15% at the absorption peak (595 nm) where the maximum is red-shifted and even broadened up to 700 nm. On the other hand, the increase in the absorption of LC state annealing-treated solar cells is only around 15% compared to untreated devices. Therefore, we presume this enhancement of the IPCE to originate from an enhancement of the charge carrier mobility because of fewer defects in the LC phase as a result of self-healing process.[30] The maximum of the IPCE at wavelength near 580 nm dramatically decreases at the annealing temperature above liquid-crystalline state (250 °C). The improved IPCE at 250 °C at 400 nm can be explained by arrangement of the polyfluorene backbone transforming into a crystalline form,[31] and the low IPCE at 600 nm is due to the disorder of DTBT.

Measurements of the total absorption spectrum and the IPCE of the PFcbpDTBT:PCBM solar cells enable the calculation of the internal quantum efficiency (IQE) spectrum shown in Figure 12B.[32] The IQE of 200 °C annealing cell (green line) nearly approaches 30% around 600 nm and stays near or even above 20% throughout the entire absorption spectrum (400−650 nm). The effects of annealing treatment on IQE of the devices is the similar to those on IPCE; that is, the LC annealing treatment favors the high IQE.

Device current density/voltage ($J-V$) characteristics based on the liquid-crystalline conjugated polymer PFcbpDTBT blending with $PC_{60}BM$ at different temperatures are shown in Figure 13, and the parameters are listed in Table 2. As expected, the annealing temperatures affect mainly the short circuit current density (J_{sc}) and fill factor (FF) with the open-circuit voltage (V_{oc}) remaining almost unchanged. This notion is supported by the morphology and molecular orbital studied of the PFcbpDTBT:$PC_{60}BM$ films upon thermal treatments. As a consequence, the power conversion efficiencies (PCE) experiences a significantly increase from 0.335% to 1.10% with an increase in the annealing temperature from room temperature to liquid-crystalline phase. Although the efficiencies of PFcbpDTBT:PCBM devices still can and need to be further improved with respect to high-end applications, the preliminary results can be comparable with that of the optimized performance polymer solar cell based on PFDTBT:PCBM.

Table 2. Characteristic Current−Voltage Parameters of Polymer Solar Cells Based on PFcbpDTBT:PCBM = 1:3 at Various Thermal Treatments

	V_{oc} (V)[a]	J_{sc} (mA/cm^2)[b]	FF[c]	PCE (%)
PFcbpDTBT	0.69	1.35	0.36	0.335
PFcbpDTBT(120)[d]	0.68	1.72	0.42	0.491
PFcbpDTBT(200)	0.68	3.38	0.48	1.10
PFcbpDTBT(250)	0.70	2.46	0.40	0.689

[a] V_{oc} is the open-circuit voltage. [b] J_{sc} is the short-circuit current. [c] The fill factor (FF) is a graphic measure of the squareness of the $I-V$ curve. [d] The number in parentheses following the copolymer represented as the annealing temperatures.

CONCLUSION

We have intramolecularly incorporated the mesogenic cyanobiphenyl to the fluorene unit in the D−A copolymer PFDTBT for the purpose of self-organization of liquid-crystalline conjugated materials. The PFcbpDTBT containing cyanobiphenyl shows red-shifted absorption bands than the pristine PFDTBT, suggesting that the incorporation of mesogenic pendants could enhance the orientation degree of the polymer and cyanobiphenyl fine-tune the energy levels. Study of the relation between the annealing conditions and the nanostructures of the polymer has revealed that the liquid crystallinity heat treatment can assemble into the most ordered lamella structure. When the PFcbpDTBT:PCBM annealed at temperature below the solid−mesophase transition, the less ordered copolymer chains bring an undeveloped interpenetrating networks. However, if the temperature is raised above the mesophase−isotropic transition, the isotropic polymer cause the large size of PCBM domains. Particularly, in the mesophase, the spontaneously self-organization of PFcbpDTBT enhance the crystallinity and orientation of the PCBM. Without extended optimization, the resulting nanoscale phase separation of the film mixtures leads to well-connected percolated networks, improving the maximum IQE to 29% at 592 nm and the PCE to 1.10% of the device.

ASSOCIATED CONTENT

Supporting Information. Text giving the experimental details, synthesis of the monomers and polymers, instrumentation, fabrication details, and characterization procedures of the PSC devices, figures showing the NMR spectrum, and TGA curve. This material is available free of charge via the Internet at http://pubs.acs.org.

AUTHOR INFORMATION

Corresponding Author

*Tel +86 791 3969562; fax +86 791 3969561; e-mail ywchen@ncu.edu.cn (Y.C.), chenlienc@163.com (L.C.), lfan@ncu.edu.cn (F.L.).

ACKNOWLEDGMENT

This work was supported by the National Natural Science Foundation of China (51073076, 50902067, and 51003045) and the National Basic Research Program (973 program) (2009CB-825104-X).

REFERENCES

(1) (a) Wurthner, F.; Meerholz, K. *Chem.—Eur. J.* **2010**, *16*, 9366–9373. (b) Thompson, B. C.; Frechet, J. M. J. *Angew. Chem., Int. Ed.* **2008**, *47*, 58–77. (c) Cheng, Y.-J.; Yang, S.-H.; Hsu, C.-S. *Chem. Rev.* **2009**, *109*, 5868–5923.

(2) Arias, A. C.; MacKenzie, J. D.; Stevenson, R.; Halls, J. J.; Inbasekaran, M. M.; Woo, E. P.; Richards, D.; Friend, R. H. *Macromolecules* **2001**, *34*, 6005–6013.

(3) (a) Beaupr, S.; Boudreault, P.-L. T.; Leclerc, M. *Adv. Mater.* **2010**, *22*, E6–E27. (b) Chen, X.; Schulz, G. L.; Han, X.; Zhou, Z.; Holdcroft, S. *J. Phys. Chem. C* **2009**, *113*, 8505–8512.

(4) (a) Inganas, O.; Svensson, M.; Zhang, F.; Gadisa, A.; Persson, N. K.; Wang, X.; Andersson, M. R. *Appl. Phys. Lett.* **2004**, *79*, 31. (b) Svensson, M.; Zhang, F. L.; Veenstra, S. C.; Verhees, W. J. H.; Hummelen, J. C.; Kroon, J. M.; Inganas, O.; Andersson, M. R. *Adv. Mater.* **2003**, *15*, 988–991.

(5) Kitazawa, D.; Watanabe, N.; Yamamoto, S.; Tsukamoto, J. *Appl. Phys. Lett.* **2009**, *95*, 053701.

(6) (a) Coropceanu, V.; Cornil, J.; da Silva Filho, D. A.; Olivier, Y.; Silbey, R.; Bredas, J. L. *Chem. Rev.* **2007**, *107*, 926–952. (b) Chen, L.-M.; Xu, Z.; Hong, Z.; Yang, Y. *J. Mater. Chem.* **2010**, *20*, 2575–2598.

(7) Brédas, J.-L.; Norton, J. E.; Cornil, J.; Coropceanu, V. *Acc. Chem. Res.* **2009**, *42*, 1691–1699.

(8) (a) Campoy-Quiles, M.; Ferenczi, T.; Agostinelli, T.; Etchegoin, P. G.; Kim, Y.; Anthopoulos, T. D.; Stavrinou, P. N.; Bradley, D. D. C.; Nelson, J. *Nature Mater.* **2008**, *7*, 158–164. (b) Bechara, R.; Leclerc, N.; Leveque, P.; Richard, F.; Heiser, T.; Hadziioannou, G. *Appl. Phys. Lett.* **2008**, *93*, 013306. (c) Mihailetchi, V. D.; Xie, H. X.; de Boer, B.; Popescu, L. M.; Hummelen, J. C.; Blom, P. W. M.; Koster, L. J. A. *Appl. Phys. Lett.* **2006**, *89*, 012107.

(9) (a) Camaioni, N.; Garlaschelli, L.; Geri, A.; Maggini, M.; Possamai, G.; Ridolfi, G. *J. Mater. Chem.* **2002**, *12*, 2065–2070. (b) Li, G.; Shrotriya, V.; Yao, Y.; Yang, Y. *J. Appl. Phys.* **2005**, *98*, 043704. (c) Erb, T.; Zhokhavets, U.; Gobsch, G.; Raleva, S.; Stuhn, B.; Schilinsky, P.; Waldauf, C.; Brabec, C. J. *Adv. Funct. Mater.* **2005**, *15*, 1193–1196.

(10) (a) McCulloch, I.; Heeney, M.; Bailey, C.; Genevicius, K.; MacDonald, I.; Shkunov, M.; Sparrowe, D.; Tierney, S.; Wagner, R.; Zhang, W.; Chabinyc, M. L.; Kline, R. J.; McGehee, M. D.; Toney, M. F. *Nature Mater.* **2006**, *5*, 328–333. (b) DeLongchamp, D. M.; Kline, R. J.; Lin, E. K.; Fischer, D. A.; Richter, L. J.; Lucas, L. A.; Heeney, M.; McCulloch, I.; Northrup, J. E. *Adv. Mater.* **2007**, *19*, 833–837. (c) Wang, L.; Cho, H.; Lee, S.; Lee, C.; Jeong, K.; Lee, M. *J. Mater. Chem.* **2011**, *21*, 60–64.

(11) Yao, K.; Chen, Y.; Chen, L.; Zha, D.; Li, F.; Pei, J.; Liu, Z.; Tian, W. *J. Phys. Chem. C* **2010**, *114*, 18001–18011.

(12) (a) Colladet, K.; Fourier, S.; Cleij, T. J.; Lusten, L.; Gelan, J.; Vanderzande, D.; Nguyen, L. H.; Neugebauer, H.; Sariciftci, S.; Aguirre, A.; Janssen, G.; Goovaerts, E. *Macromolecules* **2007**, *40*, 65–72. (b) Thompson, B. C.; Kim, Y. G.; Reynolds, J. R. *Macromolecules* **2005**, *38*, 5359–5362.

(13) (a) Kokudo, H.; Sato, T.; Yamamoto, T. *Macromolecules* **2006**, *39*, 3959. (b) Ong, B. S.; Wu, Y.; Liu, P.; Gardner, S. *J. Am. Chem. Soc.* **2004**, *126*, 3378–3379.

(14) (a) Yamamoto, T.; Kokudo, H.; Kobashi, M.; Sakai, Y. *Chem. Mater.* **2004**, *16*, 4616–4618. (b) Chen, T. A.; Wu, X.; Rieke, R. D. *J. Am. Chem. Soc.* **1995**, *117*, 233–244.

(15) Kim, D. H.; Lee, B.-L.; Moon, H.; Kang, H. M.; Jeong, E. J.; Park, J.; Han, K.-M.; Lee, S.; Yoo, B. W.; Koo, B. W.; Kim, J. Y.; Lee, W. H.; Cho, K.; Becerril, H. A.; Bao, Z. *J. Am. Chem. Soc.* **2009**, *131*, 6124–6132.

(16) (a) Nishizawa, T.; Hadykesuma, L.; Tajima, K.; Hashimoto, K. *J. Am. Chem. Soc.* **2009**, *131*, 2464–2465. (b) Ichimura, K. *Chem. Rev.* **2000**, *100*, 1847–1873.

(17) Wong, H. M. P.; Wang, P.; Abrusci, A.; Svensson, M.; Andersson, M. R.; Greenham, N. C. *J. Phys. Chem. C* **2007**, *111*, 5244–5249.

(18) McCullough, R. D.; Tristram-Nagle, S.; Williams, S. P.; Lowe, R. D.; Jayaraman, M. *J. Am. Chem. Soc.* **1993**, *115*, 4910–4911.

(19) (a) Han, P.; Cheuk, K. K. L.; Kwok, H. S.; Tang, B. Z. *Macromolecules* **2004**, *37*, 6408–6417. (b) Tang, B. Z.; Kong, X.; Wan, X.; Peng, H.; Lam, W. Y.; Feng, X.-D.; Kwok, H. S. *Macromolecules* **1998**, *31*, 2419–2432.

(20) (a) Yuan, W. Z.; Tang, L.; Zhao, H.; Jin, J. K.; Sun, J. Z.; Qin, A.; Xu, H. P.; Liu, J.; Yang, F.; Zheng, Q.; Chen, E.; Tang, B. Z. *Macromolecules* **2009**, *42*, 52–61. (b) Olsen, B. D.; Gu, X.; Hexemer, A.; Gann, E.; Segalman, R. A. *Macromolecules* **2010**, *43*, 6531–6534.

(21) (a) Huang, J. H.; Yang, C. Y.; Ho, Z. Y.; Kekuda, D.; Wu, M. C.; Chien, F. C.; Chen, P.; Chu, C. W.; Ho, K. C. *Org. Electron.* **2009**, *10*, 27–33. (b) Tsao, H. N.; Cho, D.; Andreasen, J. W.; Rouhanipour, A.; Breiby, D. W.; Pisula, W.; Mullen, K. *Adv. Mater.* **2009**, *21*, 209–212.

(22) Inganas, O.; Zhang, F.; Andersson, M. R. *Acc. Chem. Res.* **2009**, *42*, 1731–1739.

(23) (a) Scharber, M. C.; Wuhlbacher, D.; Koppe, M.; Denk, P.; Waldauf, C.; Heeger, A. J.; Brabec, C. L. *Adv. Mater.* **2006**, *18*, 789–794. (b) Ko, S.; Mondal, R.; Risko, C.; Lee, J. K.; Hong, S.; McGehee, M. D.; Bredas, J. L.; Bao, Z. *Macromolecules* **2010**, *43*, 6685–6698.

(24) (a) Po, R.; Maggini, M.; Camaioni, N. *J. Phys. Chem. C* **2010**, *114*, 695–706. (b) Ma, W.; Yang, C. Y.; Gong, X.; Lee, K.; Heeger, A. J. *Adv. Funct. Mater.* **2005**, *15*, 1617–1622.

(25) Erb, T.; Zhokhavets, U.; Gobsch, G.; Raleva, S.; Stuhn, B.; Schilinsky, P.; Waldauf, C.; Brabec, C. J. *Adv. Funct. Mater.* **2005**, *15*, 1193–1196.

(26) Chan, S. H.; Hsiao, Y. S.; Hung, L. I.; Hwang, G. W.; Chen, H. L.; Ting, C.; Chen, C. P. *Macromolecules* **2010**, *43*, 3399–3405.

(27) Yang, X.; Loos, J.; Veenstra, S. C.; Verhees, W. J.; Wienk, H. M. M.; Kroons, J. M.; Michels, M. A. J.; Janssen, R. A. J. *Nano Lett.* **2005**, *5*, 579–583.

(28) De, S.; Pascher, T.; Maiti, M.; Jespersen, K. G.; Kesti, T.; Zhang, F. L.; Inganas, O.; Yartsev, A.; Sundstrom, V. *J. Am. Chem. Soc.* **2007**, *129*, 8466–8472.

(29) Wen, S.; Pei, J.; Zhou, Y.; Li, P.; Xue, L.; Li, Y.; Xu, B.; Tian, W. *Macromolecules* **2009**, *42*, 4977–4984.

(30) (a) Padinger, F.; Rittberger, R. S.; Sariciftci, N. S. *Adv. Funct. Mater.* **2003**, *13*, 85–88. (b) Maunoury, J. C.; Howse, J. R.; Turner, M. L. *Adv. Mater.* **2007**, *19*, 805–809. (c) Funahashi, M.; Zhang, F.; Tamaoki, N. *Adv. Mater.* **2007**, *19*, 353–358.

(31) Yang, S.-H.; Hsu, C.-S. *J. Polym. Sci., Part A: Polym. Chem.* **2009**, *47*, 2713–2733.

(32) Slooff, L. H.; Veenstra, S. C.; Kroon, J. M.; Moet, D. J. D.; Sweelssen, J.; Koetse, M. M. *Appl. Phys. Lett.* **2007**, *90*, 1435061.